




Impact of ionic composition of groundwater on oxidative iron precipitation

D. Vries ^{a,*}, M. Korevaar ^b, L. de Waal ^b and A. Ahmad^c

^aWater Technology, KWR Watercycle Research Institute, Groningehaven 7, Nieuwegein 3430 BB, Netherlands

^bKWR Water Research Institute, Netherlands

^cSibelco, Netherlands

*Corresponding author. E-mail: dirk.vries@kwrwater.nl

 DV, 0000-0003-2920-5926; MK, 0000-0001-7414-6238; LdW, 0000-0001-6267-1713

ABSTRACT

In the Netherlands, approximately 60% of drinking water is obtained from (generally anaerobic) groundwater. This requires aeration followed by rapid sand filtration (RSF) to remove iron, manganese, arsenic and ammonium. The mechanisms responsible for their removal or the clogging of RSFs and breakthrough of colloidal iron or manganese oxides have not been fully elucidated in previous studies. In this work, factors affecting iron precipitation have been studied in an aerated, continuously stirred bench scale jar experiments to simulate the supernatant layer of submerged sand filters. Time series data of filtered iron concentration and precipitate size have been collected in experiments with synthetic groundwater with and without P, Si, HCO₃ and Ca at neutral pH. We show that precipitate growth is not influenced by different HCO₃ concentrations but is reduced drastically when NOM is present and, to lesser extent, Si as well. The addition of P appears to hamper precipitate growth to some extent, but requires more research. We also observe that addition of Ca improves the growth of Fe precipitates in the presence of Si and especially NOM. These results have great significance for improving Fe removal efficiency of groundwater treatment plants in Netherlands and abroad.

Key words: groundwater treatment, iron oxidation, precipitation, rapid sand filtration

HIGHLIGHTS

- Different HCO₃ concentrations have no significant impact on the precipitation of Fe for typical groundwater conditions.
- Silicate additions in the presence of HCO₃ result in reduced Fe precipitation.
- Addition of NOM in the presence of HCO₃, hamper the precipitation growth of Fe.
- The impact of Ca on precipitate growth is stronger for DOC containing water compared to Si containing water for typical concentration ranges.

INTRODUCTION

In the Netherlands, 60% of drinking water is obtained by treating groundwater, mostly by aeration and rapid sand filtration to remove impurities such as iron (Fe), manganese (Mn), arsenic (As) and ammonium (NH₄⁺). Drinking water in the Netherlands is generally of high quality, however in some cases discolouration events due to incomplete removal of Fe from groundwater are reported. Therefore, this study is focused on improving the efficiency of groundwater treatment for effective Fe removal.

When anaerobic groundwater is aerated at water treatment plants e.g. by cascades, oxygen (O₂) diffuses into groundwater and facilitates oxidation of dissolved Fe(II) to insoluble Fe(III)(oxyhydr)oxide precipitates. The Fe(III)(oxyhydr)oxide precipitates are typically removed in submerged rapid sand filters (Beek *et al.* 2015; Vries *et al.* 2016). The ionic composition of groundwater has a major impact on the structure, crystallinity and aggregation behaviour of these Fe(III) precipitates. Previous studies have shown that at near-neutral pH, Fe(II) oxidation by O₂ leads to the formation of moderately crystalline Fe(III) precipitates, such as lepidocrocite, whereby the presence of oxyanions such as silicate (Si), phosphate (P) and arsenate ((As(V)) in water leads to the formation of poorly ordered Fe(III) phases (Voegelin *et al.* 2010; van Genuchten *et al.* 2014a; Senn *et al.* 2015). The presence of oxyanions during Fe(III) precipitation not only affect the local coordination and ordering in the Fe(III) precipitates, but also decrease the extent of particle aggregation due to a highly negative surface charge which

This is an Open Access article distributed under the terms of the Creative Commons Attribution Licence (CC BY-NC-ND 4.0), which permits copying and redistribution for non-commercial purposes with no derivatives, provided the original work is properly cited (<http://creativecommons.org/licenses/by-nc-nd/4.0/>).

causes repulsion between the particles. This may result in stable colloidal suspensions, especially in solutions devoid of Ca and Mg cations, which are difficult to clarify by sedimentation and/or filtration. Bivalent cations such as Ca and Mg can counteract this repulsion effect of negative particle surface charge and can enhance particle aggregation (Senn *et al.* 2015, 2019; Ahmad *et al.* 2020). Calcium is also known as a dominant coagulating agent for solutions containing NOM and other ions (Sholkovitz & Copland 1981) and is expected to compete with trace metals for binding with NOM (Tipping 1993; van den Hoop *et al.* 1995).

In the Netherlands, the ionic composition of groundwater significantly varies from one groundwater source to another. The impact of variations in key groundwater solutes, including bicarbonate (HCO_3^-), Si, P, NOM and Ca on Fe(III) precipitation and removal at groundwater treatment plants is not yet fully understood. Most groundwater treatment systems are still designed on rules of thumb without detailed understanding of physicochemical processes. Although the oxidation and precipitation and subsequent aggregation and coagulation of Fe, see e.g. (Sholkovitz & Copland 1981; Jarvis *et al.* 2006; Bratby 2016) has been studied before, the rate of precipitation in relation to variations in the composition of groundwater has not received much attention. The residence time in groundwater treatment installations and the half-life of Fe(II) oxidation are comparable (Stumm & Morgan 1996; Vries *et al.* 2016). Hence, we believe that the investigation of the kinetics of Fe(III) precipitation due to Fe(II) oxidation are critical for improving the efficiency of rapid sand filters. To this aim, we qualitatively investigate the influence of HCO_3^- , NOM, Si, Ca and P on the rate of precipitation of Fe when oxidizing Fe(II) in simulated groundwater matrices. The ionic composition of these matrices, i.e. HCO_3^- , NOM, Si, Ca and P concentration, is derived from averaging the groundwater quality in the Netherlands. The scope of this work encompasses the influence of typical (oxy)anions and cations on iron precipitation within a bicarbonate buffered solution. To investigate the precipitation kinetics in the supernatant layer of a submerged sand filter, we use a laboratory simulated environment through the use of an aerated, continuously stirred bench scale jar experiments. It is expected that, in line with what has been published (Jobin & Ghosh 1972a), alkalinity should not impact Fe(II) oxidation at neutral pH, while Ca should have a positive effect on the Fe precipitation rate while Si, P and NOM should have a negative effect (Tipping 1993; van den Hoop *et al.* 1995).

MATERIALS AND METHODS

Initial solutions

Iron oxidation and precipitation rate experiments were performed with different initial solutions (Table 1), produced by dosing chemical stocks in ultrapure water (Milli-Q, produced by purifying distilled water with a Purelab Chorus provided by Veolia). All the initial solutions contained 80.5 μM Fe(II), 8.2 μM Mn(II), 0.60 μM As(III) and 460 μM NaCl, but differed in the concentration of HCO_3^- (1,500–300 μM), Si (320–640 μM), P (15 μM), DOC (150–300 μM) and Ca (450–1,800 μM) (See Table 1). These differences in ionic composition were chosen to simulate groundwater quality in the Netherlands. For preparing the stock solutions, reagent grade chemicals were used. Stock solutions of 22.4 g/L $\text{FeSO}_4 \cdot 7\text{H}_2\text{O}$ (CAS: 10025-77-1, 97% purity, J.T Baker The Netherlands), NaHCO_3 (CAS: 144-55-8, >99% purity, J.T Baker The Netherlands), NaCl (CAS: 7647-14-5, 99% purity, J. T Baker The Netherlands) and $\text{Na}_2\text{SiO}_3 \cdot 5\text{H}_2\text{O}$ (CAS: 10213-79-3, 99% purity, Sigma-Aldrich) respectively in ultrapure water. The stock solutions of 49.8 g/L CaCl_2 and 1.0 g/L NaH_2PO_4 were prepared by dissolving CaCl_2 anhydrous (CAS: 10043-52-4, 96% purity, J. T Baker) and $\text{NaH}_2\text{PO}_4 \cdot \text{H}_2\text{O}$ (CAS: 10049-21-5, >98% purity, J.T Baker) respectively in 0.1 M HCl. The NOM stock solution of 2.4 g/L DOC was prepared by diluting a primary stock (HumVi, Vitens, The Netherlands, 117.4 g/L DOC) that contained approximately 75% humic substances (HS) (Ahmad *et al.* 2020), see the composition in Table S1, supplementary material. Arsenic was dosed using a stock solution of 1.0 g/L As_2O_3 (CAS: 1327-53-3, 99% purity, Inorganic Ventures). For pH adjustment, 0.1 M HCl or 0.1 M NaOH is used.

Iron oxidation and precipitation experiments

Iron oxidation and precipitation rate experiments were performed with a 5 liter glass vessel connected to a controller (ez-Control, Applikon[®] Biotechnology) for adjusting, maintaining and logging (BioXpertV2 software) the pH, temperature, air supply and stirring speed (Figure 1). The experiments were carried out at pH 7.0 and 20 °C, with stirring set to 300 rpm for the first 5 minutes and 80 rpm for the rest of the experiment. The experimental procedure included: (i) preparation of the initial solutions in the oxygen-depleted reaction vessel and collection of solution samples for control, (ii) O_2 dosing to allow precipitation of Fe(III) while the suspension was stirred and (iii) collection of suspension samples after 30 minutes,

Table 1 | Composition of the initial solutions used in the precipitation experiments

Impact of ion(s)	Experimental code	Concentration ($\mu\text{mol/L}$)				
		HCO ₃	Si	P	DOC	Ca
HCO ₃	1500HCO ₃	1,475				
	1800HCO ₃	1,844				
	2200HCO ₃	2,213				
	2600HCO ₃	2,581				
	3000HCO ₃	2,950				
Oxyanions	2200HCO ₃ + 320Si	2,213	320			
	2200HCO ₃ + 640Si	2,213	641			
	2200HCO ₃ + 15P	2,213		15		
	2200HCO ₃ + 150DOC	2,213			150	
HCO ₃ + Ca	1500HCO ₃ + 900Ca	1,475	0			898
	2200HCO ₃ + 900Ca	2,213	0			898
	3000HCO ₃ + 900Ca	2,950	0			898
HCO ₃ + oxyanion + Ca	2200HCO ₃ + 320Si + 450 Ca	2,213	320			449
	2200HCO ₃ + 320Si + 900Ca	2,213	320			898
	2200HCO ₃ + 320Si + 1800Ca	2,213	320			1,796
	2200HCO ₃ + 150DOC + 900Ca	2,213			150	898
	2200HCO ₃ + 300DOC + 900Ca	2,213			300	898

In all the initial solutions the concentration of Fe(II), Mn(II) and As(III) was 81, 8.2 and 0.6 μM . All the initial solutions also contained 460 μM NaCl.

which were filtered over 0.20 μm filters (SpartanTM 30/0.20 RC 0.20 μm syringe filters (GE Healthcare, Buckinghamshire, UK)) to determine the removal of Fe(III) precipitates and co-precipitated species. The removal of Fe was determined from the difference between the measured values of the initial solution and final filtered solution.

Fe, Mn, As, Ca, Si, P were measured by Inductively Coupled Plasma Mass Spectrometry (ICP-MS) (XSERIES 2, Thermo Fisher Scientific, The Netherlands) using the collected samples before supplying air to the vessel ($t = 0$ min.) and after 30 minutes. Samples for analysis by ICP-MS were preserved immediately after collection by dosing 50 μL 65% HNO₃ per 50 mL sample and stored at 4 °C. The analysis of DOC in water samples was carried out with a TOC-V_{CPH} total organic carbon analyser (Shimadzu Benelux, 's-Hertogenbosch, The Netherlands). The samples for DOC analysis were conserved immediately after collection by adding 200 μL 30% HCl solution to 100 mL of sample which was closed off airtight and stored at 4 °C. Bicarbonate was analysed by a colorimetric method (HI-3811, Hanna Instruments) using HI 775-26 fresh water alkalinity reagent.

Particle characterization

The size and volume fraction of the precipitates was determined during the experiments by Multiple Light Scattering (MLS) using the Mastersizer 2000 (Malvern Instruments, UK). The MLS device was connected to the reaction vessel (Figure 1) and the suspension was continuously drawn through the Mastersizer measurement cell at a constant flow of 216 mL/min using a Masterflex easy-load II peristaltic pump combination (Metrohm Nederland B.V. The Netherlands). Malvern instruments Mastersizer 2000 software v5.61 recorded the particle size distribution every 20 s, for the complete duration of the experiment (30 min). A scattering coefficient¹ of 2.9 was used to determine the particle size of Fe(III)(oxyhydr)oxide particles (Gregory 2009). From the light scattering data, relative precipitate volume and the size distribution have been determined. The relative precipitate volume is the ratio of the volume of the precipitate with respect to the total volume of the measurement cell. It is assumed that detected particles do not represent Fe(III)(oxyhydr)oxide particles if the diameter of 50% percent of the particles (i.e. d₅₀) is larger than 300 μm . This threshold is selected based on the observation that the diameter of 90% of the

¹ The scattering coefficient is a measure of the ability of particles to scatter photons out of a directed beam of light. This can be related to the particle's size.

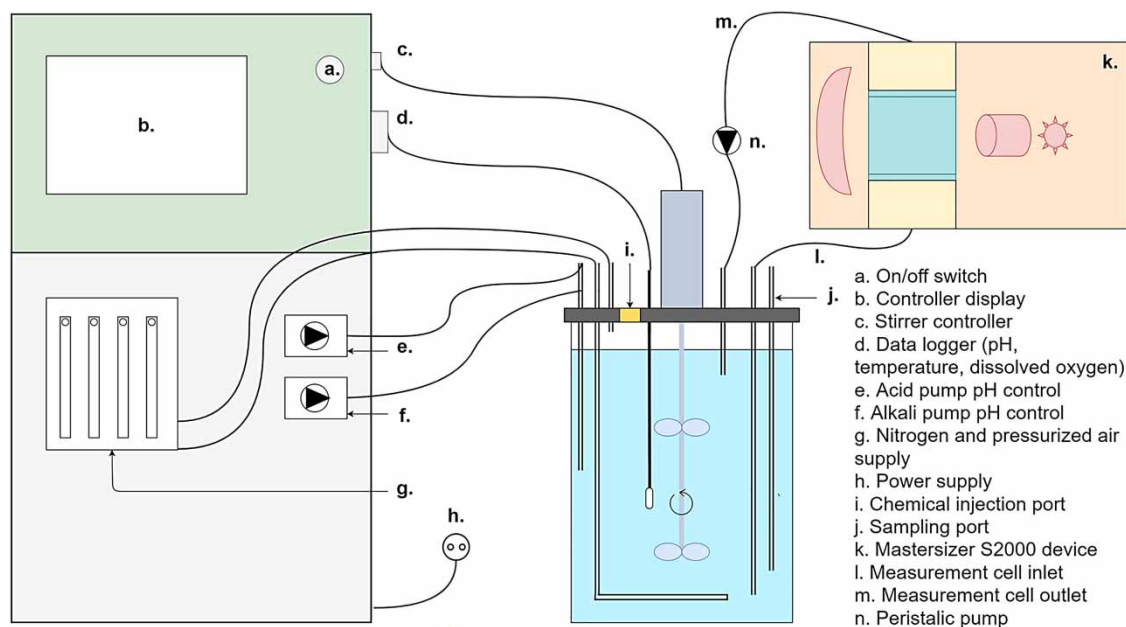


Figure 1 | A schematic overview of the experimental set-up.

particles (i.e. d_{90}) never exceeds $300\ \mu\text{m}$. The relative precipitate volume and d_{50} are omitted from the results at the times this particle size threshold is exceeded.

RESULTS AND DISCUSSION

Impact of bicarbonate

The percentage of residual Fe after filtration through a $0.20\ \mu\text{m}$ filter and the relative precipitate volume as a function of different HCO_3^- concentrations are shown in Figure 2(a) and 2(b) respectively. Figure 2(a) shows that residual Fe quickly depletes by oxidation and reaches to complete absence for all the HCO_3^- concentrations in approximately 7 minutes. The relative precipitate volume appears to stabilize in approximately 15 minutes for all the HCO_3^- concentrations, except that of $1,500\ \mu\text{M}$

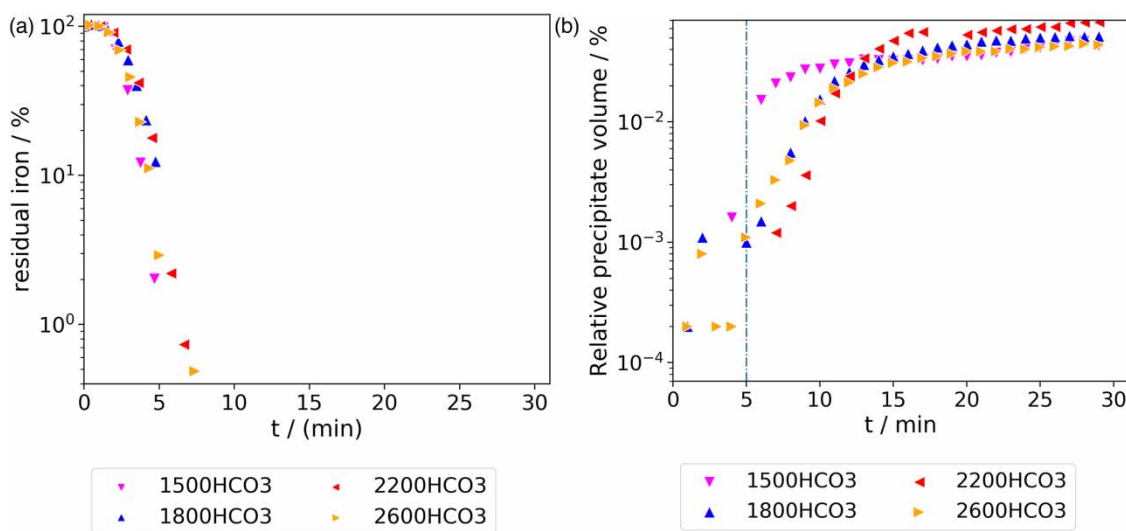


Figure 2 | (a) Residual iron (%) after filtration through a $0.2\ \mu\text{m}$ filter and (b) precipitate volume relative to the total measured volume, as a function of different HCO_3^- concentrations.

HCO_3^- which is the lowest HCO_3^- concentration. At this concentration the relative precipitate volume stabilizes already in 7 minutes. The particle size show the same trend as the relative precipitate volume, i.e. the d_{50} reaches approximately 100 μm after 30 minutes (Figure S1-A, supplementary material). These results are in agreement with the findings of (Jobin & Ghosh 1972b) who showed that Fe(II) oxidation is only hampered when the buffer intensity is sufficiently large (i.e. in the order of $4 \cdot 10^{-3} \text{ eq CaCO}_3/\text{pH}$, hence an alkalinity of more than 16 mmol/L as HCO_3^- at neutral pH, which is substantially higher than the highest HCO_3^- concentration of 2,600 $\mu\text{mol/L}$ used in this study. These results show that different HCO_3^- concentrations have no significant impact on the precipitation of Fe and precipitation is completed quite rapidly when the typical residence times of 15–30 minutes for groundwater treatment plants are considered.

Impact of oxyanions and natural organic matter

The percentage of residual Fe after filtration through 0.20 μm filter and the relative precipitate volume as a function of different Si, P and NOM concentrations in the presence of 2,200 μM HCO_3^- are shown in Figure 3(a) and 3(b) respectively. Figure 3(a) shows that the percentage of residual Fe concentration stays approximately 100% for most samples, i.e. no significant Fe removal was observed except for the 30 min sample of 15 μM P addition. In all cases, the relative precipitation volume (Figure 3(b)) signal was also unstable, indicating a poor Fe precipitation. The poor Fe precipitation and reduced size of Fe particles due to Si additions are in agreement with previous studies (Liu *et al.* 2007; Piispanen & Sallanko 2011; Kinsela *et al.* 2016; Li *et al.* 2019). Silicate ions bind strongly to Fe(III) precipitate surfaces during Fe(III) polymerization, which modifies two key properties of the suspension. Firstly, by binding strongly to crystal growth sites on the Fe(III) precipitate surface, oxyanions inhibit the formation of crystalline Fe(III) minerals (i.e. lepidocrocite), leading to formation of poorly-ordered Fe(III) precipitates with a large specific surface area (Voegelin *et al.* 2010; van Genuchten *et al.* 2014b). Secondly, sorption of Si leads to negatively charged Fe(III) precipitate surfaces (Kanematsu *et al.* 2013; Delaire *et al.* 2016). Therefore, the sorption of Si leads to particles having a highly negative surface charge that are less likely to aggregate. Indeed, small amounts of Si are removed (Supplementary Table S2). The work of Piispanen *et al.* shows empirically that if the molar Si/Fe ratio exceeds 2.5, extremely small sized Fe particles are formed. In our study, the molar ratio of Si/Fe in the initial solution was in the range of 4–8, thus much higher. The particle size at $t = 30$ minutes is 7–10 μm after 30 minutes, hence an order of magnitude smaller than the case without Si (Figure S1-B, supplementary material).

Our observations related to NOM additions are in agreement with several previous studies which also report a similar reduction in the removal of Fe(III) in the presence NOM (Vilg -Ritter *et al.* 1999; Davis & Edwards 2017; Ahmad *et al.* 2019). The suppression of Fe(III) removal by filtration has been attributed to formation of soluble Fe(III)–NOM complexes, as well as formation of Fe(III)–NOM and Fe(III)(oxyhydr)oxide–NOM colloids. However, the characterisation of the particles (Fe(III)–NOM or Fe(III)(oxyhydr)oxide–NOM colloids) was not investigated in our study, hence properties of the soluble fractions of Fe(III)–NOM complexes remain unclear. Also, it is known that the presence of $\text{Ca} + 2$ (or $\text{Mg} + 2$)

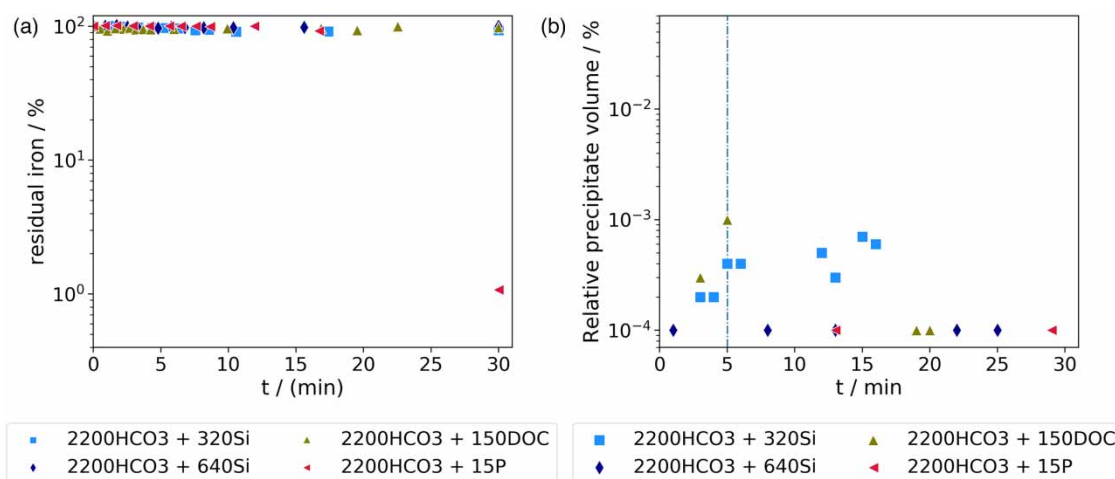


Figure 3 | (a) Residual iron (%) after filtration through a 0.2 μm filter and (b) precipitate volume relative to the total measured volume, as a function of different Si, P and NOM concentrations in the presence of 2,200 μM HCO_3^- .

suppresses electrostatic repulsion forces between humic acid-Fe colloids and hence accelerate aggregation (Liao *et al.* 2017) and part of this effect can be seen when comparing Figure 3 with Figure 4. Table S1 shows the characterization of NOM. Note that the influence of different NOM compositions can have a different impact on precipitation (Sharp *et al.* 2006), these impacts were not studied in this work.

Regarding the behaviour of P in our study, sequential precipitation of different Fe(III) phases could be responsible for the initial stability and later destabilization of the suspension at 30 min to result in a lower residual Fe concentration after 0.20 μm filtration. In previous studies of Fe(II) oxidation in the presence of P, precipitation of Lp-like material has been observed due to the sequential uptake of P during precipitate formation (Voegelin *et al.* 2010, 2013; van Genuchten *et al.* 2014a, 2014b; Senn *et al.* 2015, 2018). With the initial P/Fe(II) molar ratio of 0.55 (critical ratio) or higher, only P gets removed from the solution and Fe(II) oxidation will lead to exclusive formation of amorphous Fe(III)-phosphate. However, with an initial P/Fe < critical P/Fe as is the case in our study where P/Fe is 0.2, multiple phases can be formed. These phases include the precipitation of polymeric Fe(III)-phosphate, and after the depletion of P from the solution, the formation of more crystalline iron oxide phases (Senn *et al.* 2018). The identity of the iron oxide formed after P depletion strongly depends on oxyanions in water. In oxyanion-free electrolytes such as our study formation of lepidocrocite is likely which could have caused the particle growth in the 30 min sample. Nevertheless, we conclude that more investigations are required to understand the P related observations from our study.

Impact of calcium

The % of residual Fe after filtration through 0.20 μm filter and relative precipitate volume as a function of different HCO_3^- , Si, P NOM concentrations in the presence of Ca are shown in Figure 4(a) and 4(b) respectively. The results in Figure 4(a) show that at constant Ca concentration of 900 μM , the efficiency of Fe removal decreases with increasing HCO_3^- concentration. Without calcium, the removal was complete within 10 minutes for the HCO_3^- additions (Figure 2(a)), but with the addition of 900 μM Ca the time to complete removal of Fe by 0.20 μm increases up to 30 minutes. These results needs further investigations to unravel the mechanisms responsible for this peculiar impact of Ca on Fe precipitation in the presence of HCO_3^- .

The addition of 450–1,800 μM Ca in $\text{HCO}_3^- + \text{Si}$ solutions appears to slightly lower the residual Fe concentration (compare Figures 3(a) and 4(a)), potentially attributed to charge neutralization and subsequent precipitate aggregation effect that the Ca ions create for the Si containing disordered Fe(III)(oxyhydr)oxides (Voegelin *et al.* 2010). Particles do hardly grow in size however, reaching to approximately 1–2 μm after 30 minutes (Figure S1-C, supplementary material). The addition of Ca in the presence of 150–300 μM DOC significantly improves the removal of Fe by 0.2 μm filters, indicating effective growth and aggregation of the Fe(III), see Figure 4 and Figure S1-C (supplementary material) for the relative precipitate volume and d_{50} respectively. These results are in agreement with previous studies (Sholkovitz & Copland 1981; Knocke *et al.* 1994). This can be explained based on the influence of DOC and Ca on the surface charge of the Fe precipitates. Because the NOM used in this study is largely composed of negatively charged humic substances, its complexation with Fe precipitates will increase the negative charge of the surface, thus hampering precipitate growth. However, when Ca is present in the solution, it can bind with these DOC-Fe complexes and reduce the surface charge to promote precipitate growth as was also seen

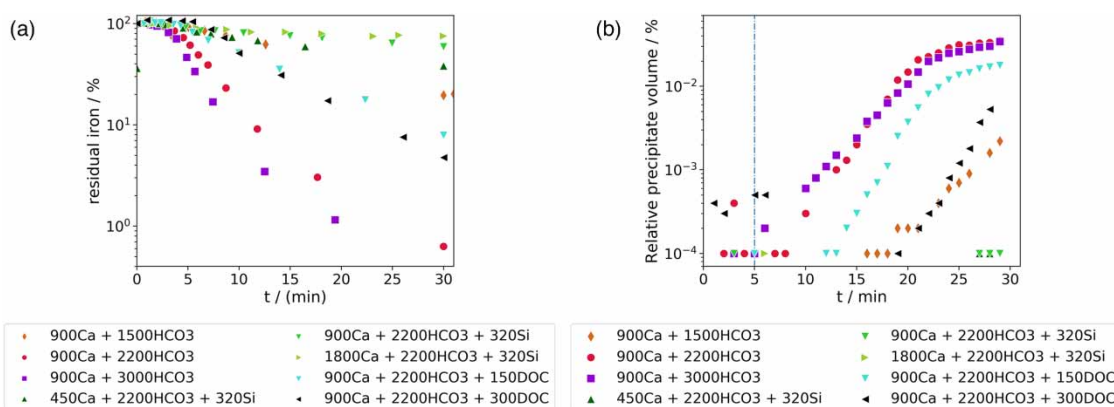


Figure 4 | (a): residual iron (%) after passing through a 0.2 μm filter and (b) precipitate volume relative to the total measured volume, both shown as time series. See Table 1: for explanation of the labels.

in e.g. the work of (Liao *et al.* 2017). Note that Si and DOC are filtered out, together with Fe (supplementary material Table S2). Moreover, no calcium was removed by this filtering.

The implications of this study for groundwater treatment practice could be manifold. First, an expected increase in rain fall due to climate change, can cause the mobilization of NOM in drinking water sources, leading to increased levels of dissolved organic matter (DOM) and humic substances, alterations to their structure and reactivity (Lipczynska-Kochany 2018). Lipczynska-Kochany also anticipates increased desorption from soil and sediments, as well as re-mobilization of metals and organic pollutants. In addition, the increased levels of acidic atmospheric CO₂ participates increasingly in the weathering of carbonate and silicate minerals, leading to more bicarbonate, Ca⁺² and other cations in drinking water sources (Qafoku 2015). While a change in only bicarbonate does not alter (Fe) precipitation dynamics, changes calcium concentration does. This could be exploited by water utility operators for further optimisation of the iron removal efficiency. Moreover, precipitation dynamics are tightly linked with oxidation dynamics. As a result of the pre-aeration step in rapid sand filtration treatment, anaerobic groundwater containing Fe(II) oxidises via Fe(III) into Fe(hydr)oxides even in the absence of suspended particles or any other complexation agents by homogeneous chemical kinetics, also known as homogeneous oxidation (Davison & Seed 1983; Moses & Herman 1989). An auto-catalytic process, so-called heterogeneous oxidation, occurs if suspended precipitates allow for sorption and surface complexation with ferrous iron ions (Sung & Morgan 1980; Stumm & Sulzberger 1992; Sharma 2001). Heterogeneous oxidation is a dominant process in the removal of Fe by RSFs (Wolthoorn *et al.* 2004; Vries *et al.* 2016), but becomes retarded when P, Si or humic substances are present (Wolthoorn *et al.* 2004). Hence, (also) ionic strength and oxyanions can affect the rate of heterogeneous oxidation as well as the charge of Fe(III) (hydroxy)oxide precipitates, and leads to altered precipitation and coagulation characteristics.

Concluding, depending on aquifer characteristics and mineral weathering, the current operation of groundwater treatment sites might be in need of evaluation and further investigation whether additional measures are needed to keep Fe and other metal ion levels in drinking water at an acceptable level. For instance, in groundwater coming from calcareous soils, elevated levels of Ca and HCO₃ enhances precipitation of Fe and coagulation of humic substances. Possible softening of the treated groundwater could therefore lead to a more effective overall treatment when placed after RSF and carry-over filtering and also allow reuse of calcite granules when calcite pellet contactors are used (Schettlers *et al.* 2014; Tang *et al.* 2019). For optimisation of drinking water production and water source management under changing conditions, it is necessary to investigate the mechanisms that underpin the interplay of precipitation, colloidal stability and oxidation to arrive at an evidence based plant operation. This requires, amongst others, that the relation between precipitation rate and water composition as shown in this paper, needs to be quantified to eventually capture that in a model.

CONCLUSIONS AND IMPLICATIONS

We studied the precipitation of Fe in simulated groundwater solutions with different concentrations of HCO₃, Si, P, NOM and Ca, reflecting typical groundwater quality conditions in the Netherlands. We conclude that the different HCO₃ concentrations have no significant impact on the precipitation of Fe and precipitation is completed in the typical residence time of groundwater treatment plants. Silicate additions in the presence of HCO₃ result in reduced Fe precipitation, probably because of the negatively charged silicate-iron co-precipitate surfaces because this hampers precipitate growth. The additions of NOM in the presence of HCO₃, drastically hamper the precipitation growth of Fe, potentially due to the formation of soluble Fe(III)-NOM complexes. Phosphate and bicarbonate containing solutions initially hamper precipitate growth but more work is needed to conclude something definitive on the impact of P on Fe precipitation dynamics. Addition of Ca improves Fe precipitate growth in the presence of Si and NOM, potentially attributed to charge neutralization impact of Ca.

These results clearly indicate that, when designing RSF for iron removal, attention should be paid to the whole water matrix. Moreover, mineral weathering is accelerated by climate change and causes rising Ca and DOC levels of current drinking water sources. Consequently, monitoring of water compositional changes and iron removal is needed to assess whether operational measures in RSF groundwater treatment should be taken.

ACKNOWLEDGEMENTS

This research is financed by the Joint Research Programme of the Dutch Water Companies (BTO). Discussions with and feedback from the members of the project steering committee, i.e. Stephan van de Wetering, Simon Dost, Frank Schoonenberg,

Ben Cools, and Alexander Rohling, have contributed to this work and are highly appreciated. We would like to thank prof. Emile Cornelissen (KWR, UGent) and the anonymous reviewers for their critical review of the paper.

DATA AVAILABILITY STATEMENT

All relevant data are included in the paper or its Supplementary Information.

REFERENCES

- Ahmad, A., van der Wal, A., Bhattacharya, P. & van Genuchten, C. M. 2019 Characteristics of Fe and Mn bearing precipitates generated by Fe(II) and Mn(II) co-oxidation with O₂, MnO₄ and HOCl in the presence of groundwater ions. *Water Res.* **161**, 505–516. <https://doi.org/10/gh9376>.
- Ahmad, A., Rutten, S., Eikelboom, M., de Waal, L., Bruning, H., Bhattacharya, P. & van der Wal, A. 2020 Impact of phosphate, silicate and natural organic matter on the size of Fe(III) precipitates and arsenate co-precipitation efficiency in calcium containing water. *Sep. Purif. Technol.* **235**, 116117. <https://doi.org/10/ggf86k>.
- Beek, C. v., Dusseldorp, J., Joris, K., Huysman, K., Leijssen, H., Schoonenberg-Kegel, F., de Vet, W., van de Wetering, S. & Hofs, B. 2015 Contributions of homogeneous, heterogeneous and biological iron (II) oxidation in aeration and rapid sand filtration (RSF) in field sites. *J. Water Supply Res. Technol.* Aqua jws2015059.
- Bratby, J. 2016 *Coagulation and Flocculation in Water and Wastewater Treatment*. IWA Publishing.
- Davis, C. C. & Edwards, M. 2017 Role of calcium in the coagulation of NOM with ferric chloride. *Environ. Sci. Technol.* **51**, 11652–11659. <https://doi.org/10/gm5hdq>.
- Davison, W. & Seed, G. 1983 The kinetics of the oxidation of ferrous iron in synthetic and natural waters. *Geochim. Cosmochim. Acta* **47**, 67–79. <https://doi.org/10/dbwfr4>.
- Gregory, J. 2009 Optical monitoring of particle aggregates. *J. Environ. Sci.* **21**, 2–7. <https://doi.org/10/d2v3md>.
- Jarvis, P., Jefferson, B. & Parsons, S. A. 2006 Floc structural characteristics using conventional coagulation for a high doc, low alkalinity surface water source. *Water Res.* **40**, 2727–2737. <https://doi.org/10/c33jnp>.
- Jobin, R. & Ghosh, M. M. 1972a Effect of buffer intensity and organic matter on the oxygenation of ferrous iron. *J. Am. Water Works Assoc.* **64**, 590–595. <https://doi.org/10/gftfhh>.
- Jobin, R. & Ghosh, M. M. 1972b Effect of buffer intensity and organic matter on the oxygenation of ferrous iron. *J. Am. Water Works Assoc.* **64**, 590–595.
- Kinsela, A. S., Jones, A. M., Bligh, M. W., Pham, A. N., Collins, R. N., Harrison, J. J., Wilsher, K. L., Payne, T. E. & Waite, T. D. 2016 Influence of dissolved silicate on rates of Fe(II) oxidation. *Environ. Sci. Technol.* **50**, 11663–11671. <https://doi.org/10/f9ddb5>.
- Knocke, W. R., Shorney, H. L. & Bellamy, J. D. 1994 Examining the reactions between soluble iron, DOC, and alternative oxidants during conventional treatment. *J. - Am. Water Works Assoc.* **86**, 117–127. <https://doi.org/10/gftfhv>.
- Li, B., Trueman, B. F., Rahman, M. S., Gao, Y., Park, Y. & Gagnon, G. A. 2019 Understanding the impacts of sodium silicate on water quality and iron oxide particles. *Environ. Sci. Water Res. Technol.* **5**, 1360–1370. <https://doi.org/10/gm5hcq>.
- Liao, P., Li, W., Jiang, Y., Wu, J., Yuan, S., Fortner, J. D. & Giammar, D. E. 2017 Formation, aggregation, and deposition dynamics of NOM-iron colloids at anoxic–oxic interfaces. *Environ. Sci. Technol.* **51**, 12235–12245. <https://doi.org/10/gm5hdg>.
- Lipczynska-Kochany, E. 2018 Effect of climate change on humic substances and associated impacts on the quality of surface water and groundwater: a review. *Sci. Total Environ* **640–641**, 1548–1565. <https://doi.org/10/gjnz2x>.
- Liu, R., Qu, J., Xia, S., Zhang, G. & Li, G. 2007 Silicate hindering *In Situ* formed ferric hydroxide precipitation: inhibiting arsenic removal from water. *Environ. Eng. Sci.* **24**, 707–715. <https://doi.org/10/cx2mmd>.
- Moses, C. O. & Herman, J. S. 1989 Homogeneous oxidation kinetics of aqueous ferrous iron at circumneutral pH. *J. Solut. Chem.* **18**, 705–725. <https://doi.org/10/d6ndps>.
- Piispanen, J. K. & Sallanko, J. T. 2011 Effect of silica on iron oxidation and floc formation. *J. Environ. Sci. Health Part A* **46**, 1092–1101. <https://doi.org/10/ghh35m>.
- Qafoku, N. P. 2015 Chapter two – climate-change effects on soils: accelerated weathering, soil carbon, and elemental cycling. In: *Advances in Agronomy* (Sparks, D. L., ed.). Academic Press, pp. 111–172. <https://doi.org/10.1016/bs.agron.2014.12.002>.
- Schetters, M. J. A., van der Hoek, J. P., Kramer, O. J. I., Kors, L. J., Palmen, L. J., Hofs, B. & Koppers, H. 2014 Circular economy in drinking water treatment: reuse of ground pellets as seeding material in the pellet softening process. *Water Sci. Technol.* **71**, 479–486. <https://doi.org/10/f64858>.
- Senn, A.-C., Kaegi, R., Hug, S. J., Hering, J. G., Mangold, S. & Voegelin, A. 2015 Composition and structure of Fe(III)-precipitates formed by Fe(II) oxidation in water at near-neutral pH: interdependent effects of phosphate, silicate and Ca. *Geochim. Cosmochim. Acta* **162**, 220–246. <https://doi.org/10/gm5hdm>.
- Senn, A.-C., Hug, S. J., Kaegi, R., Hering, J. G. & Voegelin, A. 2018 Arsenate co-precipitation with Fe(II) oxidation products and retention or release during precipitate aging. *Water Res.* **131**, 334–345. <https://doi.org/10/gc27rs>.
- Sharma, S. K. 2001 *Adsorptive Iron Removal From Groundwater*. IHE Delft, Wageningen University, Delft, The Netherlands.

- Sharp, E. L., Jarvis, P., Parsons, S. A. & Jefferson, B. 2006 Impact of fractional character on the coagulation of NOM. *Colloids Surf. Physicochem. Eng. Asp.* **286**, 104–111. <https://doi.org/10/cxhfkf>.
- Sholkovitz, E. R. & Copland, D. 1981 The coagulation, solubility and adsorption properties of Fe, Mn, Cu, Ni, Cd, Co and humic acids in a river water. *Geochim. Cosmochim. Acta* **45**, 181–189. <https://doi.org/10/fbs5qw>.
- Stumm, W. & Morgan, J. J. 1996 *Aquatic Chemistry: Chemical Equilibria and Rates in Natural Waters*. Wiley-Interscience.
- Stumm, W. & Sulzberger, B. 1992 The cycling of iron in natural environments: considerations based on laboratory studies of heterogeneous redox processes. *Geochim. Cosmochim. Acta* **56**, 3233–3257. <https://doi.org/10/c4srmh>.
- Sung, W. & Morgan, J. J. 1980 Kinetics and product of ferrous iron oxygenation in aqueous systems. *Environ. Sci. Technol.* **14** (5), 561–568. <https://doi.org/10.1021/es60165a006>.
- Tang, C., Jørgensen Hedegaard, M., Lopato, L. & Albrechtsen, H.-J. 2019 Softening of drinking water by the pellet reactor – effects of influent water composition on calcium carbonate pellet characteristics. *Sci. Total Environ.* **652**, 538–548. <https://doi.org/10/gjn2q5>.
- Tipping, E. 1993 Modeling the competition between alkaline earth cations and trace metal species for binding by humic substances. *Environ. Sci. Technol.* **27**, 520–529. <https://doi.org/10/fcdjb7>.
- van den Hoop, M. A. G. T., van Leeuwen, H. P., Pinheiro, J., Mota, A. M. & Simões Gonçalves, M. d. L. 1995 Voltammetric analysis of the competition between calcium and heavy metals for complexation by humic material. *Colloids Surf. Physicochem. Eng. Asp.* **95**, 305–313. <https://doi.org/10/fbzxtj>.
- van Genuchten, C. M., Gadgil, A. J. & Peña, J. 2014a Fe(III) nucleation in the presence of bivalent cations and oxyanions leads to subnanoscale 7 Å polymers. *Environ. Sci. Technol.* **48**, 11828–11836. <https://doi.org/10/f6mmj8>.
- van Genuchten, C. M., Peña, J., Amrose, S. E. & Gadgil, A. J. 2014b Structure of Fe(III) precipitates generated by the electrolytic dissolution of Fe(0) in the presence of groundwater ions. *Geochim. Cosmochim. Acta* **127**, 285–304. <https://doi.org/10/f5px5f>.
- Vilgé-Ritter, A., Rose, J., Masion, A., Bottero, J.-Y. & Lainé, J.-M. 1999 Chemistry and structure of aggregates formed with Fe-salts and natural organic matter. *Colloids Surf. Physicochem. Eng. Asp.* **147**, 297–308. <https://doi.org/10/d8fkhh>.
- Voegelin, A., Kaegi, R., Frommer, J., Vantelon, D. & Hug, S. J. 2010 Effect of phosphate, silicate, and Ca on Fe(III)-precipitates formed in aerated Fe(II)- and As(III)-containing water studied by X-ray absorption spectroscopy. *Geochim. Cosmochim. Acta* **74**, 164–186. <https://doi.org/10/bvbnm6>.
- Voegelin, A., Senn, A.-C., Kaegi, R., Hug, S. J. & Mangold, S. 2013 Dynamic Fe-precipitate formation induced by Fe(II) oxidation in aerated phosphate-containing water. *Geochim. Cosmochim. Acta* **117**, 216–231. <https://doi.org/10/f49k2c>.
- Vries, D., Bertelkamp, C., Schoonenberg-Kegel, F., Hofs, B., Dusseldorp, J., Bruins, J., de Vet, W. & van den Akker, B. 2016 Iron and manganese removal: recent advances in modelling treatment efficiency by rapid sand filtration. *Water Res.*, 35–45. <https://doi.org/10/gftf3g>.
- Wolthoorn, A., Temminghoff, E. J., Weng, L. & van Riemsdijk, W. H. 2004 Colloid formation in groundwater: effect of phosphate, manganese, silicate and dissolved organic matter on the dynamic heterogeneous oxidation of ferrous iron. *Appl. Geochem.* **19**, 611–622. <https://doi.org/10/fpn7mm>.

First received 6 July 2021; accepted in revised form 14 November 2021. Available online 29 November 2021